*Int. J. Electrochem. Sci.*, 17 **(2022)** Article Number: 220635, doi: 10.20964/2022.06.22

International Journal of
ELECTROCHEMICAL
SCIENCE
www.electrochemsci.org

*Short Communication*

# Photocatalytic Reduction of Chromium(VI) in Wastewater by Ag/WO3/rGO Nanocomposite under Visible Light Irradiation

*Lixiu Liu*[*], *Aijiang He, Xia Yao*

School of New Materials and Chemical Energy, Yibin Vocational Technical College, Yibin 644003, China
[*]E-mail: Liulixiu2020@163.com

*Received:* 16 February 2022 / *Accepted:* 29 March 2022 / *Published:* 7 May 2022

Under visible light irradiation, a photocatalytic reduction of hexavalent chromium (Cr(VI)) in wastewater was demonstrated using an Ag/$WO_3$/rGO nanocomposite. The nanocomposite was created using a hydrothermal technique. The integration of Ag nanoparticles and rGO nanosheets into the $WO_3$ structure resulted in increased porosity and roughness, as well as enhanced active sites on the surface of the nanocomposite, which can improve the effective surface area, according to structural analyses using XRD and SEM. Based on UV–vis absorption spectra, the optical band-gaps of $WO_3$, Ag/$WO_3$, and Ag/$WO_3$/rGO nanocomposite were predicted to be 2.89, 2.80, and 2.59 eV, respectively. Electrochemical investigations revealed that the Ag/$WO_3$/rGO nanocomposite exhibited a lower electrochemical resistance to charge transfer than $WO_3$ and Ag/$WO_3$, indicating efficient charge transportation and decreased photo-generated carrier recombination kinetics. Photocatalytic analyses revealed that after 120, 95, and 80 minutes of visible light irradiation, respectively, 90 percent removal efficiency of Cr(VI) ions was obtained, whereas complete removal of $WO_3$, Ag/$WO_3$, and Ag/$WO_3$/rGO nanocomposite was obtained after 155, 130, and 120 minutes of visible light irradiation, respectively. The practical ability of Ag/$WO_3$/rGO nanocomposite to reduce Cr(VI) in prepared genuine samples of industrial wastewater was examined, and the results demonstrated the suggested photocatalyst's efficient performance in reducing Cr(VI) in industrial wastewater.

**Keywords:** Ag/$WO_3$/rGO; Nanocomposite; Hydrothermal; Hexavalent chromium; Photocatalytic reduction

## 1. INTRODUCTION

Chromium (Cr) is a valuable heavy metal and a raw material used in the alloy industry to harden steel and produce stainless steel [1-3]. Cr plating can be used to give steel a polished mirror quality and to improve corrosion resistance, hardness, and aesthetics [4-6]. Chromium compounds are also employed as industrial catalysts, pigments, printing inks, copper dyeing, glass, and cement [7-9].

Electroplating, tanning, pharmaceuticals, fuel and oxidants, and matches are only a few of the applications [10-12].

Cr is a potentially harmful metal, and contamination of groundwater by Cr may occur as a result of Cr leaching from land-based solid waste disposal due to insufficient storage or industrial waste disposal techniques [13-15]. Cr(VI) is formed naturally in the environment when natural Cr deposits erode. Cr(VI) is a common skin sensitizer, causing dermatitis, allergic and eczematous skin reactions, skin and mucous membrane ulcerations, allergic asthmatic reactions, bronchial carcinomas, and gastro-enteritis [16]. Inhaled Cr(VI) has been demonstrated in studies to be a human carcinogen, increasing the incidence of lung cancer and lung tumors [17-19].

As a result, many studies have been conducted to develop techniques for removing Cr(VI) from wastewaters using biological treatment, reduction and filtration, adsorption, ion exchange, electrodialysis, coagulation, electrochemical treatment, and photocatalysis, among other methods [20-22]. Among these treatment techniques, photocatalytic reduction of Cr(VI) is a low-cost method that uses the semiconductors and light source to formation the photo-excited electron as strong reducing agents and free radicals [23-25]. However, issues such as high recombination rates of photogenerated charge carriers and low utilization of solar energy as an inexhaustible source of renewable energy have been observed in photocatalytic systems, preventing commercialization [26, 27]. As a result, researchers have been working on developing new nanostructured martial arts in order to improve the potential application of photocatalytic systems in visible light and reduce the recombination rate of photogenerated charge carriers [28-30]. Therefore, the present work demonstrated a strong photocatalytic reduction of Cr(VI) in wastewater by $Ag/WO_3$/rGO nanocomposite under visible light irradiation.

## 2. EXPERIMENTAL

### *2.1. Synthesis of $Ag/WO_3$/rGO nanocomposites*

A hydrothermal technique was applied to synthesize $Ag/WO_3$/rGO nanocomposite as the following process [31]: 50 ml of 0.5 M $Na_2WO_4.2H_2O$ (99.0%, Sigma-Aldrich) aqueous solution, 10 ml of nitric acid (65%, Dongying Qihao Chemical Co., Ltd., China) was added and magnetically stirred to obtain a yellow homogeneous suspension. The yellow homogeneous suspension was then added to 70 ml of 5mM $AgNO_3$ (99.0%, Sigma-Aldrich) solution and magnetically agitated for 60 minutes. The suspension was then placed in a 200 mL Teflon-lined stainless steel autoclave and heated to 200°C for 12 hours. The precipitates were collected after cooling, washed with deionized water, and filtered three times with deionized water using filter paper (20 m, Whatman). The filtered precipitates were dried at 90 °C for 12 hours, and subsequently ground to achieve the homogenous $Ag/WO_3$ powder. For the synthesis of the $Ag/WO_3$/rGO nanocomposite, 250 mg of $Ag/WO_3$ powder was ultrasonically added to 10 ml of 5 g/l graphene oxide suspension (Sigma-Aldrich). The ultrasonication was continued for 10 minutes to achieve a homogeneous suspension. Next, the obtained suspension was transferred into the 200 ml Teflon-lined stainless steel autoclave at 190°C for 12 hours. After the

hydrothermal process, the resultant precipitates were rinsed three times with deionized water and ethanol. Finally, the obtained Ag/WO3/rGO nanocomposite was dried in the oven at 80 °C for 10 hours.

### *2.2. Instrumental analytical methods*

The crystal structure of the samples was examined using X-Ray diffraction (XRD; XPERT PRO-Analytical, Netherlands), and the wavelength of the source CuK used was 1.54060. The morphological examination of nanostructures was carried out using scanning electron microscopy (SEM; HITACHI S4800, Japan). A UV-vis spectrophotometer was used to measure absorption spectra (Cary 5000, Agilent, Santa Clara, CA, USA). EIelectrochemical impedance spectroscopy (EIS) experiments were carried out under visible light illumination, to compare electron transfer rate in photocatlysts at frequency range from $10^{-1}$ to$10^{6}$ Hz and AC voltage 10 mV in 0.5 M Na2SO4 (≥99%, Sigma-Aldrich) solution using a potentiostat/galvanostat (Autolab® model PGSTAT 10N, Eco Chemie, Netherland) and electrochemical cell which contained $WO_3$, Ag/$WO_3$ and Ag/$WO_3$/rGO nanocomposite modified glassy carbon electrode (GCE) as working electrode, saturated Ag/AgCl electrode as a reference electrode and a platinum plate as counter electrode. The EIS data was fitted using equivalent circuits with ZView software. For the preparation of the modified GCE surface with $WO_3$, Ag/$WO_3$ and Ag/$WO_3$/rGO nanocomposite, 20 g/l of synthesized nanostructures suspension was mixed with 1 ml of dimethylformamide (DMF, 99.9%, Dongying Qihao Chemical Co., Ltd., China), and dropped on the GCE surface and dried at room temperature.

The photocatalytic reduction of Cr(VI) was performed in a test chamber which contained 0.5 g/1 photocatalyst ($WO_3$ or Ag/$WO_3$ or Ag/$WO_3$/rGO nanocomposite) and 200 ml of 100 mg/l Cr(VI) (≥90%, Sigma-Aldrich) solution which was prepared with deionized water, and a 150 W Xenon lamp (Hangzhou Sg Electronic Technology Co., Ltd., China) as a visible light source and located at the top of the device. The distance between the surface of Xenon lamp and the surface of Cr(VI) solution was kept constant at 5 cm. Prior to the light irradiation, the mixture of photocatalysts and Cr(VI) solution were magnetically stirred in a dark place for 60 minutes to establish the adsorption/desorption equilibrium between the Cr(VI) ions and the nanostructured photocatalysts. After irradiation visible light, irradiated samples were filtered through a filter paper (100 μm, Whatman), and concentration of the irradiated Cr(VI) solutions was estimated using UV-vis absorbance at $\lambda_{max}$ = 540 nm [32]. The photocatalytic removal efficiency was determined using the following equation [33, 34]:

$$\text{Removal efficiency (\%)} = \frac{I_0 - I_t}{I_0} \times 100 = \frac{C_0 - C_t}{C_0} \times 100 \qquad (1)$$

Where $I_o$, $C_o$, and $I_t$, $C_t$ are the absorbance intensity and corresponded concentration of the Cr(VI) at initial and after irradiation visible light at time t, respectively.

## 3. RESULTS AND DISCUSSION

### *3.1. XRD and SEM analyses*

Figures 1a, 1b, and 1c show the extent of crystallization in the form of powders for WO3, Ag/WO3, and Ag/WO3/rGO nanocomposite, respectively. Figure 1 shows the diffraction peaks of synthesized WO3 at 22.91°, 24.51°, 33.51°, and 34.25°, which could correspond to the (002), (200), (021), and (220) planes of WO3 with monoclinic phase of WO3 (JCPDS card no. 43-1035) [35]. Figure 1b shows additional peaks at 38.52°, 44.81° and 64.32° which are related to (111), (200) and (220) planes of face centered cubic (fcc) structure of Ag (JCPDS card no. 04-0783) [36], indicating incorporation of Ag nanoparticles into the $WO_3$ structure. The XRD pattern of the Ag/$WO_3$/rGO nanocomposite in Figure 1c also displays the additional peaks at 10.51° which correspond to (001) planes of GO [37-39].

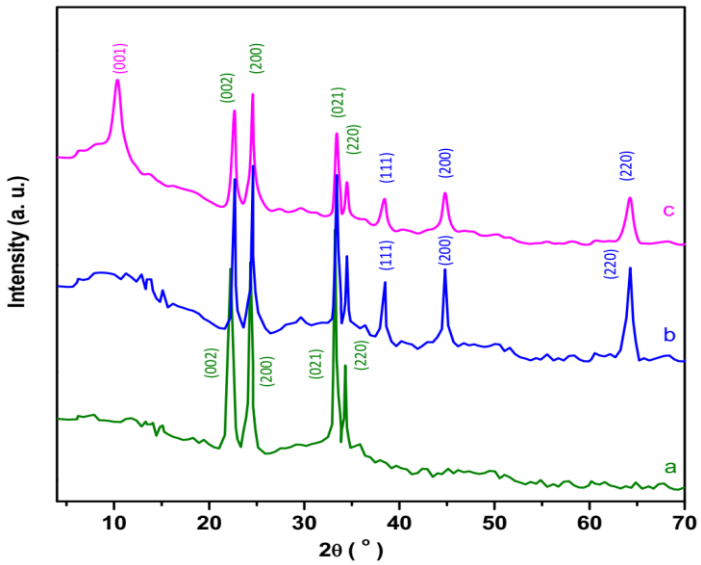


**Figure 1.** The XRD patterns of powders of (a) $WO_3$, (b) Ag/$WO_3$ and (c) Ag/$WO_3$/rGO nanocomposite.

Figure 2 shows SEM images of $WO_3$, Ag/$WO_3$, and Ag/$WO_3$/rGO nanocomposite. Figure 2a shows that $WO_3$ nanoparticles are generated in the form of nanoflakes with an average size of 30 nm. As seen in SEM images of the Ag/$WO_3$/rGO nanocomposite in Figure 2b, the Ag/WO3 nanoflakes are equally implanted across the rGO nanosheets. It has been discovered that including rGO nanosheets increases porosity and roughness, as well as creates improved active sites on the surface of the nanocomposite, hence increasing the effective surface area [40-42]. Furthermore, the findings of the XRD study and observations in SEM pictures indicate that the Ag/$WO_3$/rGO nanocomposite was successfully synthesized.

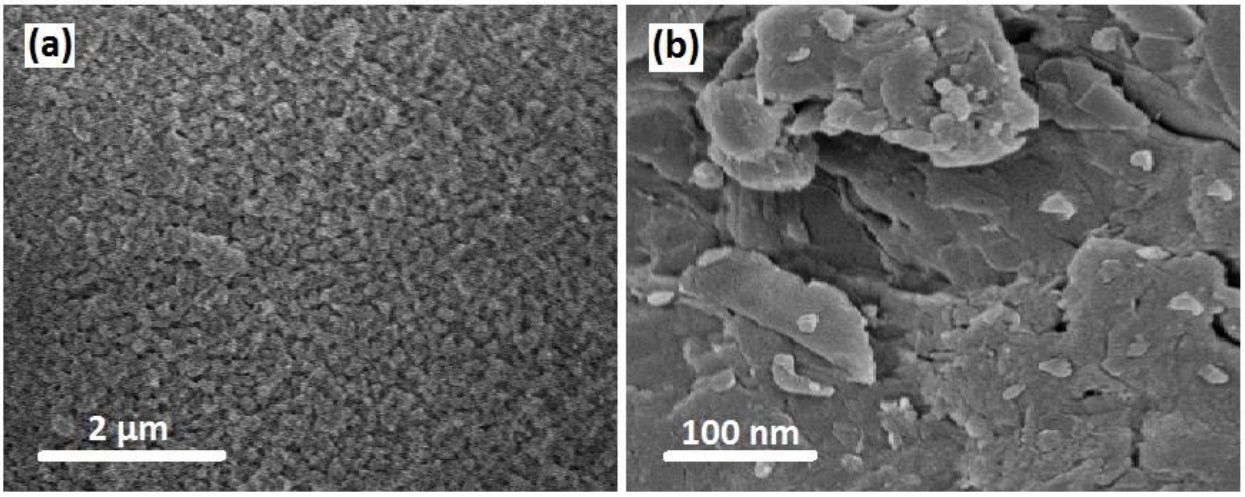


**Figure 2.** The SEM images of (a)$WO_3$, (b)Ag/$WO_3$/rGO nanocomposite.

*3.2. Optical analysis*

As shown in Figure 3a, UV–vis absorption spectroscopy was used to evaluate the optical characteristics of $WO_3$, Ag/$WO_3$, and Ag/$WO_3$/rGO nanocomposite. The absorption edges of Ag/$WO_3$ and Ag/$WO_3$/rGO nanocomposite toward $WO_3$ are slightly red-shifted and exhibit absorption edges in the visible light region, which is due to the incorporation of Ag nanoparticles and rGO nanosheet into the $WO_3$ structure creating defects states that are normally resides deep in the band gap that forms the intermediate energy level to reduce the energy of absorbed light [29, 31, 43]. Reports indicate that the restoration of the π–π conjugation network of rGO in the $WO_3$ structure leads to a red-shift of the absorption band-edges [44, 45]. As is known, semiconductor photocatalysts can be excited by light with energy higher than their optical band gap. The photo-excited electrons are generated in the valance band and then migrate to the conduction band. The addition of Ag nanoparticles and rGO nanosheets to the $WO_3$ structure causes the formation of oxygen vacancy and trapped states which can reduce the electron-hole pair recombination rate, and can promote the photocatalytic performance of the Ag/$WO_3$/rGO nanocomposite [46, 47]. It can be explained by interaction between the Ag and $WO_3$ particles and presence of energy levels below the conduction band and above the valence band, and position of Fermi level of Ag which is below the conduction band edge of $WO_3$ [46, 48]. When the nanocomposite is irradiated with light the photo-generated electrons are trapped in oxygen vacancy sites and can jump to the conduction band, causing a decrease in the recombination rate because of electron scavenger role of the Ag atom [46, 49]. Thus, the photo-generated electrons can be effectively transferred from the conduction band of $WO_3$ to the Fermi energy of Ag. Moreover, rGO nanosheets can also act as an electron sink to capture photo-generated electrons and increase the exciton lifetime and decrease recombination of photo-generated carriers, and improve the absorption ability of the visible region [50, 51]. The band gap of synthesized nanostructures can be determined using the Kubelka's formula [52, 53]:

$$(\alpha h\nu)^2 = A(h\nu - Eg) \qquad (2)$$

Where hν and α are photon energy and absorption coefficient, respectively. A is proportionality constant and Eg is the optical band gap. As observed from Figure 4b, the Eg values can be calculated by Tauc plot which obtained by extrapolation of the linear part of $(\alpha h\nu)^2$ versus hν [54, 55]. The Eg of $WO_3$, $Ag/WO_3$ and $Ag/WO_3$/rGO nanocomposite are estimated ~2.89, 2.80 and 2.59 eV, respectively. It is observed that the values of the Eg decrease as the incorporation of Ag nanoparticles and rGO nanosheets in $WO_3$ structure, indicating an enhancement in the conductivity and absorption of visible light of the $Ag/WO_3$/rGO nanocomposite because of the effect of Ag metallic nanoparticles and rGO nanosheets as conductive materials, as well as effectively improving the internal electron density [56-58], and generating energy states within the band gap which act as intermediate steps for electrons in their transitions between the valence and conduction bands and accelerate the charge separation and transport [59, 60]. The photocatalytic activity in visible light and solar light harvesting capability of $Ag/WO_3$/rGO nanocomposite are greatly enhanced by narrowing the band gap and extending the light absorption range.

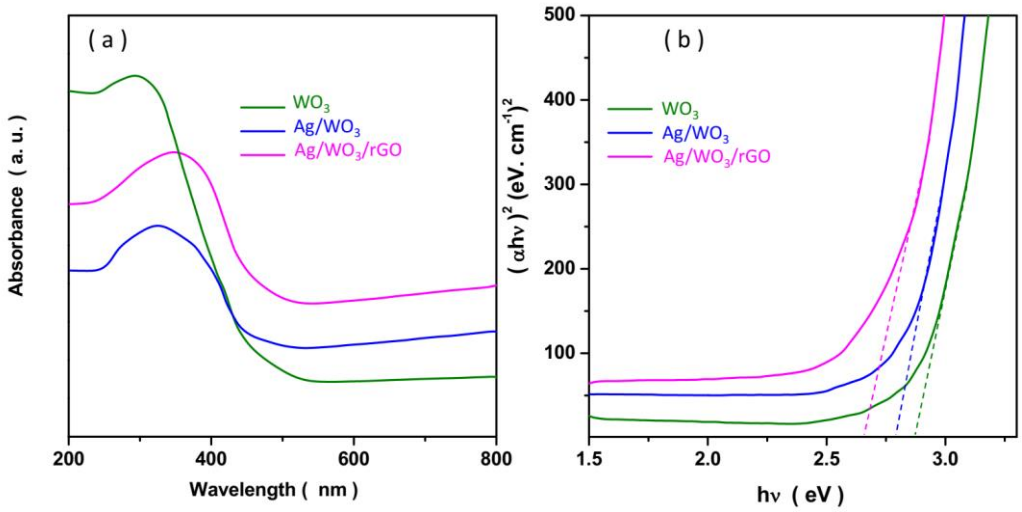


**Figure 3.** (a) UV–vis absorption spectra and (b) Tauc plot of $WO_3$, $Ag/WO_3$ and $Ag/WO_3$/rGO nanocomposite.

*3.3. Electrochemical analysis*

Figures 4a and 4b show the Nyquist and Bode plots of $WO_3$, $Ag/WO_3$, and $Ag/WO_3$/rGO nanocomposite, respectively, as well as the equivalent circuits that were used to fit and acquire the parameters listed in Table 1. The parameters include $C_1$ and $C_2$ as the counter and working electrodes' constant phase elements, $R_{c1}$ and $R_{c2}$ as the charge transfer resistance at the counter and working electrodes, respectively, and Rs as the series resistance [61, 62]. As observed, the Nyquist plots consist two arcs. The first arc corresponds to the high frequency range and is related to charge transfer resistance at the counter electrode/electrolyte interface, and the second arc is attributed to the low and middle frequency ranges, which is indicated by the impedance of the interface between the electrolyte and working electrode which ascribes the competition with the transfer of injected electrons through

the working electrode [63, 64]. As found from Table 1, the Ag/$WO_3$/rGO nanocomposite shows lower electrochemical impedance to charge transfer than that of $WO_3$ and Ag/$WO_3$, indicating efficient charge transportation and lower recombination kinetics of photo-generated carriers in the Ag/$WO_3$/rGO nanocomposite [65-67].

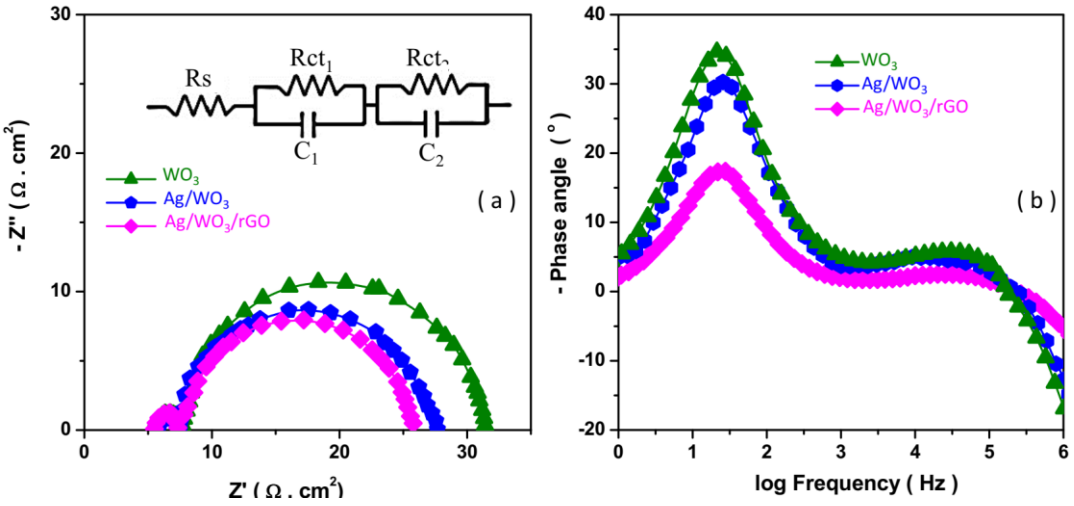


**Figure 4.** (a) Nyquist and (b) Bode plots of $WO_3$, Ag/$WO_3$ and Ag/$WO_3$/rGO nanocomposite.

**Table 1.** The obtained EIS parameters.

| **Sample** | **Rs (Ω.cm²)** | **Rct₁ (Ω.cm²)** | **Rct₂ (Ω.cm²)** |
|---|---|---|---|
| $WO_3$ | 5.80 | 2.20 | 24.53 |
| Ag/$WO_3$ | 5.90 | 2.10 | 19.35 |
| Ag/$WO_3$/rGO | 6.10 | 2.00 | 18.33 |

*3.4. Photocatalytic analyses*

Under visible light irradiation, the photocatalytic activity of $WO_3$, Ag/$WO_3$, and Ag/$WO_3$/rGO nanocomposite was tested for the elimination of 200 ml of 100 mg/l Cr(VI) solution. Figure 5 depicts removal efficiency in terms of time in darkness, visible light irradiation, and photocatalyst presence and absence. The mixture of Cr(VI) solution and photocatalysts was magnetically agitated in darkness for 60 minutes prior to the start of visible light irradiation to achieve the adsorption/desorption equilibrium between the Cr(VI) ions and the photocatalysts. Figure 5 shows that after 60 minutes, the removal effectiveness of Cr(VI) in darkness is less than 0.9%. Furthermore, after 160 minutes of visible light irradiation, the removal effectiveness is less than 1.8% in the absence of the photocatalyst. However, in the presence of photocatalysts and under visible light irradiation, the removal efficiency is

significantly increased, indicating a synergetic effect of physicalchemical properties of light and photocatalysts on the reduction of Cr(VI) [68, 69].

Furthermore, Cr(VI) ions are removed with 90% efficiency after 120, 95, and 80 minutes of visible light irradiation, respectively, whereas $WO_3$, $Ag/WO_3$, and $Ag/WO_3$/rGO nanocomposite are removed completely after 155, 130, and 120 minutes of visible light irradiation, respectively. According to SEM results, the $Ag/WO_3$/rGO nanocomposite has a higher removal efficiency and a faster treatment rate when compared to other photocatalysts. This can be attributed to the increased effective surface area due to increased porosity and roughness, as well as active sites on the nanocomposite's surface. Moreover, efficient electron-hole separation and ultra-fast electron transfer play a main role in the great photocatalytic activity of the $Ag/WO_3$/rGO nanocomposite associated with its lower band gap and more capability of visible light absorption in accordance with optical and EIS results [70, 71]. Additionally, the localized surface plasmon resonance effect of Ag nanoparticles can be excited to generate hot charge carriers, which contribute to the reduction of Cr(VI) ions in solution [72-74]. The incorporation of rGO into the $Ag/WO_3$ with great mobility of charge carriers and excellent specific surface area can also provide the possibility for effective light adsorption and high ion transfer in solution and hydroxyl radicals in the photochemical reaction [44, 75].

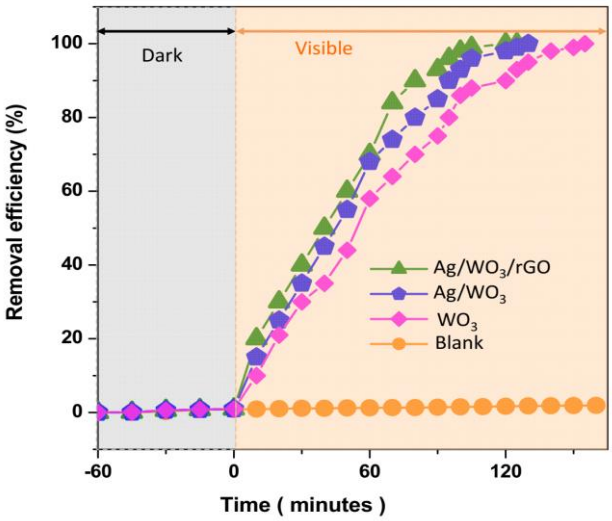


**Figure 5.** Removal efficiency in term of time for 200 ml of 100 mg/l Cr(VI) solution in darkness, under visible light irradiation and in absence (blank) and presence of photocatalysts.

Table 2 displays the performance of reported photocatalysts for Cr(VI) reduction in the literature. When comparing the photocatalytic performances of $Ag/WO_3$/rGO nanocomposite to those of other photocatalysts [76], it is clear that the synthesized nanocomposite in this study has the highest effective removal efficiency for the reduction of Cr(VI) under visible light irradiation due to the formation of an intermediate band in the energy band-gap of $WO_3$-based nanocomposite due to the addition of rGO and Ag, which increases electron density and allows for efficient

**Table 2.** Performance of reported photocatalysts in the literatures for reduction of Cr(VI) .

| **Photocatalyst** | **Cr(VI) content (mg/l)** | **Light source** | **Degradation time (minute)** | **Removal efficiency (%)** | **Ref.** |
|---|---|---|---|---|---|
| $Ag/WO_3/rGO$ | 100 | visible | 120 | 100 | This work |
| $Ag/WO_3$ | | | 130 | 100 | |
| $WO_3$ | | | 155 | 100 | |
| $TiO_2$/graphene hydrogel composite | 5 | UV | 30 | 100 | [77] |
| $TiO_2$/CdS | 10 | visible | 240 | 93 | [78] |
| $TiO_2$/rGO | 12 | visible | 240 | 86.5 | [79] |
| Titanate nanotubes | 17.7 | UV | 60 | 100 | [80] |
| $TiO_2$/CNTs | 20 | UV | 180 | 67.5 | [81] |
| dye-sensitized nanoscale ZnO | 20 | visible | 360 | 68 | [82] |
| | | | 1020 | 90 | |
| $CuBi_2O_4$–$TiO_2$ | 30 | sunlight | <240 | 98 | [83] |
| hollow $Bi_2S_3$ nanospheres | 40 | visible | 120 | 90 | [84] |
| Flower-like ZnO hollow microspheres | 246 | UV | 180 | 83 | [85] |

The potential of the $Ag/WO_3/rGO$ nanocomposite to reduce Cr(VI) in real-world industrial wastewater samples was assessed. The removal effectiveness of 100 ml of 2 mg/l Cr(VI) solutions made from deionized water and industrial effluent under visible light irradiation is shown in Figures 6a and 6b in terms of time. Because of the presence of organic and inorganic pollutants in industrial wastewater [86,87], the reduction of Cr(VI) is obtained after 25 and 45 minutes in samples prepared from deionized water and industrial wastewater, respectively, implying that the more time (20 minutes) is required for complete reduction of Cr(VI) in samples prepared from industrial wastewater. Additionally, it is also notable that colloidal particles in wastewater can reduce the photocatalytic efficiency of composites under light illumination. Furthermore, the results demonstrate the efficacy of the suggested photocatalyst in reducing Cr(VI) in industrial effluent.

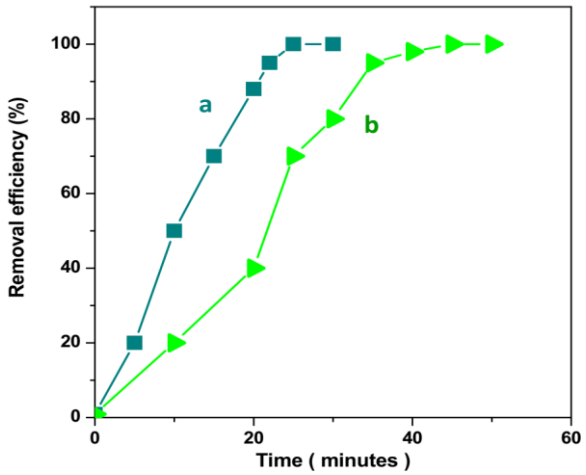


**Figure 6.** Removal efficiency of 100 ml of 2 mg/l Cr(VI) solutions in term of time for samples prepared in (a) deionized water and (b) real sample of paints and pigments industrial wastewater using $Ag/WO_3/rGO$ nanocomposite under visible light irradiation.

## 4. CONCLUSION

This research focused on hydrothermally produced Ag/$WO_3$/rGO nanocomposite and its application to photocatalytic reduction of Cr(VI) in wastewater using visible light. The structural studies revealed that Ag nanoparticles and rGO nanosheets were incorporated into the $WO_3$ framework. Based on UV–vis absorption spectra, the optical band-gaps of $WO_3$, Ag/$WO_3$, and Ag/$WO_3$/rGO nanocomposite were predicted to be 2.89, 2.80, and 2.59 eV, respectively. According to EIS results, the Ag/$WO_3$/rGO nanocomposite had a lower electrochemical impedance to charge transfer than $WO_3$ and Ag/$WO_3$, indicating efficient charge transportation and decreased recombination kinetics of photo-generated carriers in the Ag/$WO_3$/rGO nanocomposite. Photocatalytic analyses revealed that complete removal is obtained after 155, 130, and 120 minutes of visible light irradiation for $WO_3$, Ag/$WO_3$ and Ag/$WO_3$/rGO nanocomposite, respectively. The practical ability of Ag/$WO_3$/rGO nanocomposite was evaluated to reduction of Cr(VI) in prepared real samples of industrial wastewater and results illustrated to efficient performance of proposed photocatalyst for reduction of Cr(VI) in industrial wastewater.

ACKNOWLEDGMENTS
The authors are grateful for the financial support provided by the Chemical and environmental science and technology innovation team (No. ybzy20cxtd03).

## References

1. M.-T. Wu, Y.-L. Li, Q. Guo, D.-W. Shao, M.-M. He and T. Qi, *Journal of Cleaner Production*, 240 (2019) 118187.
2. L. Zhang, Y. Xu, H. Liu, Y. Li, S. You, J. Zhao and J. Zhang, *Journal of Water Process Engineering*, 44 (2021) 102368.
3. W. Liu, J. Li, J. Zheng, Y. Song, Z. Shi, Z. Lin and L. Chai, *Environmental Science & Technology*, 54 (2020)
4. J.-Z. Cheng, Z.-R. Tan, Y.-Q. Xing, Z.-Q. Shen, Y.-J. Zhang, L.-L. Liu, K. Yang, L. Chen and S.-Y. Liu, *Journal of Materials Chemistry A*, 9 (2021) 5787.
5. Z.-R. Tan, Y.-Q. Xing, J. Cheng, G. Zhang, Z.-Q. Shen, Y. Zhang, G. Liao, L. Chen and S.-Y. Liu, *Chemical Science*, 13 (2022) 1725.
6. G. Li, S. Huang, N. Zhu, H. Yuan and D. Ge, *Journal of Hazardous Materials*, 403 (2021) 123981.
7. H. Patel, *RSC Advances*, 10 (2020) 31611.
8. H. He, Q.-Q. Zhu, Y. Yan, H.-W. Zhang, Z.-Y. Han, H. Sun, J. Chen, C.-P. Li, Z. Zhang and M. Du, *Applied Catalysis B: Environmental*, 302 (2022) 120840.
9. T. Gao, C. Li, Y. Zhang, M. Yang, D. Jia, T. Jin, Y. Hou and R. Li, *Tribology International*, 131 (2019) 51.
10. W. Nabgan, A.A. Jalil, B. Nabgan, M. Ikram, M.W. Ali and P. Lakshminarayana, *Chemosphere*, 288 (2022) 132535.
11. Y. Liu, Q. Zhang, H. Yuan, K. Luo, J. Li, W. Hu, Z. Pan, M. Xu, S. Xu and I. Levchenko, *Journal of Alloys and Compounds*, 868 (2021) 158723.
12. C.-X. Chen, S.-S. Yang, J. Ding, G.-Y. Wang, L. Zhong, S.-Y. Zhao, Y.-N. Zang, J.-Q. Jiang, L. Ding and Y. Zhao, *Applied Catalysis B: Environmental*, 298 (2021) 120495.
13. C. Tsioptsias, G. Samiotis, L. Lefteri and E. Amanatidou, *Water, Air, & Soil Pollution*, 231 (2020) 1.

14. H. Liu, X. Li, Z. Ma, M. Sun, M. Li, Z. Zhang, L. Zhang, Z. Tang, Y. Yao and B. Huang, *Nano Letters*, 21 (2021) 10284.
15. Y. Liu, B. Li, X. Lei, S. Liu, H. Zhu, E. Ding and P. Ning, *Chemical Engineering Journal*, 428 (2022) 131991.
16. H. Karimi-Maleh, R. Darabi, M. Shabani-Nooshabadi, M. Baghayeri, F. Karimi, J. Rouhi, M. Alizadeh, O. Karaman, Y. Vasseghian and C. Karaman, *Food and Chemical Toxicology*, 162 (2022) 112907.
17. E.R. Braver, P. Infante and K. Chu, *Teratogenesis, carcinogenesis, and mutagenesis*, 5 (1985) 365.
18. S.-S. Yang, X.-L. Yu, M.-Q. Ding, L. He, G.-L. Cao, L. Zhao, Y. Tao, J.-W. Pang, S.-W. Bai and J. Ding, *Water research*, 189 (2021)
19. G. Li, S. Huang, N. Zhu, H. Yuan, D. Ge and Y. Wei, *Chemical Engineering Journal*, 421 (2021) 127852.
20. S. Kerur, S. Bandekar, M.S. Hanagadakar, S.S. Nandi, G. Ratnamala and P.G. Hegde, *Materials Today: Proceedings*, 42 (2021) 1112.
21. U.O. Aigbe and O.A. Osibote, *Journal of Environmental Chemical Engineering*, 8 (2020) 104503.
22. Y. Zhao, D. Kang, Z. Chen, J. Zhan and X. Wu, *International Journal of Electrochemical Science*, 13 (2018) 1250.
23. L. Zhang, L. Wang, Y. Zhang, D. Wang, J. Guo, M. Zhang and Y. Li, *Environmental research*, 206 (2022) 112629.
24. F. Chen, J. Ma, Y. Zhu, X. Li, H. Yu and Y. Sun, *Journal of Hazardous Materials*, 426 (2022) 128064.
25. L. He, M.-X. Li, F. Chen, S.-S. Yang, J. Ding, L. Ding and N.-Q. Ren, *Journal of hazardous materials*, 417 (2021) 126113.
26. M. Nazeer, F. Hussain, M.I. Khan, E.R. El-Zahar, Y.-M. Chu and M. Malik, *Applied Mathematics and Computation*, 420 (2022) 126868.
27. H. Karimi-Maleh, C. Karaman, O. Karaman, F. Karimi, Y. Vasseghian, L. Fu, M. Baghayeri, J. Rouhi, P. Senthil Kumar and P.-L. Show, *Journal of Nanostructure in Chemistry*, (2022) 1.
28. Z. Zhao, H. An, J. Lin, M. Feng, V. Murugadoss, T. Ding, H. Liu, Q. Shao, X. Mai and N. Wang, *The Chemical Record*, 19 (2019) 873.
29. R. Hassanzadeh, A. Siabi-Garjan, H. Savaloni and R. Savari, *Materials Research Express*, 6 (2019) 106429.
30. H. Wang, T. Song, Z. Li, J. Qiu, Y. Zhao, H. Zhang and J. Wang, *ACS applied materials & interfaces*, 13 (2021) 25918.
31. V.A. Tran, T.P. Nguyen, V.T. Le, I.T. Kim, S.-W. Lee and C.T. Nguyen, *Journal of Science: Advanced Materials and Devices*, 6 (2021) 108.
32. K. Joshi and V. Shrivastava, *Applied Nanoscience*, 1 (2011) 147.
33. W. Zhao, J. Zhang, F. Zhu, F. Mu, L. Zhang, B. Dai, J. Xu, A. Zhu, C. Sun and D.Y. Leung, *Chemical Engineering Journal*, 361 (2019) 1352.
34. Y.-M. Chu, B. Shankaralingappa, B. Gireesha, F. Alzahrani, M.I. Khan and S.U. Khan, *Applied Mathematics and Computation*, 419 (2022) 126883.
35. M.N. Mancheva, R.S. Iordanova, D.G. Klissurski, G.T. Tyuliev and B.N. Kunev, *The Journal of Physical Chemistry C*, 111 (2007) 1101.
36. A.S. Lanje, S.J. Sharma and R.B. Pode, *J. Chem. Pharm. Res*, 2 (2010) 478.
37. Q.T. Ain, S.H. Haq, A. Alshammari, M.A. Al-Mutlaq and M.N. Anjum, *Beilstein journal of nanotechnology*, 10 (2019) 901.
38. T.H. Zhao, M.I. Khan and Y.M. Chu, *Mathematical Methods in the Applied Sciences*, (2021) 1.
39. H. Maleh, M. Alizadeh, F. Karimi, M. Baghayeri, L. Fu, J. Rouhi, C. Karaman, O. Karaman and R. Boukherroub, *Chemosphere*, (2021) 132928.

40. H. Savaloni, E. Khani, R. Savari, F. Chahshouri and F. Placido, *Applied Physics A*, 127 (2021) 1.
41. H. Savaloni, R. Savari and S. Abbasi, *Current Applied Physics*, 18 (2018) 869.
42. J. Huo, H. Wei, L. Fu, C. Zhao and C. He, *Chinese Chemical Letters*, (2022) 1.
43. S. Ramkumar and G. Rajarajan, *Journal of Materials Science: Materials in Electronics*, 27 (2016) 12185.
44. L. Fu, T. Xia, Y. Zheng, J. Yang, A. Wang and Z. Wang, *Ceramics International*, 41 (2015) 5903.
45. M. Zhang, H. Zhu, B. Xi, Y. Tian, X. Sun, H. Zhang and B. Wu, *Processes*, 10 (2022) 301.
46. S. Ghosh, M. Saha, S. Paul and S. De, *Nanoscale*, 7 (2015) 18284.
47. S. Ren, B. Ye, S. Li, L. Pang, Y. Pan and H. Tang, *Nano Research*, 15 (2022) 1500.
48. F. Puga, J.A. Navío and M.C. Hidalgo, *Journal of Alloys and Compounds*, 867 (2021) 159191.
49. L. Jia, Y. Yu, Z.-p. Li, S.-n. Qin, J.-r. Guo, Y.-Q. Zhang, J.-C. Wang, J.-c. Zhang, B.-g. Fan and Y. Jin, *Bioresource Technology*, 332 (2021) 125086.
50. M.K. Purkait and C.-T. Chang, *International Journal of Hydrogen Energy*, 45 (2020) 17174.
51. K. Zhou, J. Xu, G. Xiao and Y. Huang, *Journal of Materials Processing Technology*, 302 (2022) 117503.
52. T. Malevu and R. Ocaya, *International Journal of Electrochemical Science*, 10 (2015) 4097.
53. D. Zhang, H. Yang, Y. Li, Z. Li, N. Gao, W. Zhou and Z. Liang, *International Journal of Electrochemical Science*, 16 (2021) 150951.
54. A. Bedia, F.Z. Bedia, M. Aillerie, N. Maloufi and B. Benyoucef, *Energy Procedia*, 74 (2015) 529.
55. N.M. Mohamed, R. Bashiri, F.K. Chong, S. Sufian and S. Kakooei, *international journal of hydrogen energy*, 40 (2015) 14031.
56. S. Zhang, J. Li, X. Wang, Y. Huang, M. Zeng and J. Xu, *Journal of Materials Chemistry A*, 3 (2015) 10119.
57. H. Khojasteh, M. Salavati-Niasari and F.S. Sangsefidi, *Journal of Alloys and Compounds*, 746 (2018) 611.
58. S. Yang, B. Xue, Y. Li, X. Li, L. Xie, S. Qin, K. Xu and Q. Zheng, *Chemical Engineering Journal*, 383 (2020) 123072.
59. X. Yu, Z. Li, K. Dang, Z. Zhang, L. Gao, L. Duan, Z. Jiang, J. Fan and P. Zhao, *Journal of Materials Science: Materials in Electronics*, 29 (2018) 8729.
60. Y. Duan, H. Fu, L. Zhang, R. Gao, Q. Sun, Z. Chen and H. Du, *Composites Communications*, 31 (2022) 101106.
61. W. Maiaugree, S. Pimanpang, W. Jarernboon and V. Amornkitbamrung, *International Journal of Photoenergy*, 2016 (2016) 1.
62. J.-S. Jia, Y. Cao, T.-X. Wu, Y. Tao, Y.-M. Pan, F.-P. Huang and H.-T. Tang, *ACS Catalysis*, 11 (2021) 6944.
63. S.C. Pradhan and S. Soman, *Results in Surfaces and Interfaces*, 5 (2021) 100030.
64. E. Alizadeh, M. Khorshidian, S.M. Rahgoshay, S.H. Masrori Saadat and M. Rahimi-Esbo, *Iranian Journal of Hydrogen & Fuel Cell*, 3 (2016) 127.
65. C.V. Reddy, I.N. Reddy, K. Ravindranadh, K.R. Reddy, D. Kim and J. Shim, *Separation and Purification Technology*, 252 (2020) 117352.
66. M. Zhang, X. Sun, C. Wang, Y. Wang, Z. Tan, J. Li and B. Xi, *Materials Chemistry and Physics*, 278 (2022) 125697.
67. Y. Wang, C. Li, Y. Zhang, M. Yang, B. Li, L. Dong and J. Wang, *International Journal of Precision Engineering and Manufacturing-Green Technology*, 5 (2018) 327.
68. M.B. Hussain, U. Azhar, H.M. Loussala and R. Razaq, *Arabian Journal of Chemistry*, 13 (2020) 5939.

69. T. Gao, C. Li, Y. Wang, X. Liu, Q. An, H.N. Li, Y. Zhang, H. Cao, B. Liu and D. Wang, *Composite Structures*, 286 (2022) 115232.
70. S. Li, J. Wang, Y. Xia, P. Li, Y. Wu, K. Yang, Y. Song, S. Jiang, T. Zhang and B. Li, *Chemical Engineering Journal*, 417 (2021) 129298.
71. J. You, C. Liu, X. Feng, B. Lu, L. Xia and X. Zhuang, *Carbohydrate Polymers*, 288 (2022) 119332.
72. C. Peng, W. Wang, W. Zhang, Y. Liang and L. Zhuo, *Applied Surface Science*, 420 (2017) 286.
73. H. Li, Y. Zhang, C. Li, Z. Zhou, X. Nie, Y. Chen, H. Cao, B. Liu, N. Zhang and Z. Said, *The International Journal of Advanced Manufacturing Technology*, (2022) 1.
74. Y.-M. Chu, U. Nazir, M. Sohail, M.M. Selim and J.-R. Lee, *Fractal and Fractional*, 5 (2021) 119.
75. D. Jia, Y. Zhang, C. Li, M. Yang, T. Gao, Z. Said and S. Sharma, *Tribology International*, 169 (2022) 107461.
76. B. Li, C. Li, Y. Zhang, Y. Wang, D. Jia and M. Yang, *Chinese Journal of Aeronautics*, 29 (2016) 1084.
77. Y. Li, W. Cui, L. Liu, R. Zong, W. Yao, Y. Liang and Y. Zhu, *Applied Catalysis B: Environmental*, 199 (2016) 412.
78. X. Liu, L. Pan, T. Lv and Z. Sun, *Journal of Alloys and Compounds*, 583 (2014) 390.
79. Y. Zhao, D. Zhao, C. Chen and X. Wang, *Journal of Colloid and Interface Science*, 405 (2013) 211.
80. W. Liu, J. Ni and X. Yin, *Water research*, 53 (2014) 12.
81. N. Shaham-Waldmann and Y. Paz, *Chemical Engineering Journal*, 231 (2013) 49.
82. G.C. Yang and S.-W. Chan, *Journal of Nanoparticle Research*, 11 (2009) 221.
83. H. Lahmar, M. Benamira, F.Z. Akika and M. Trari, *Journal of Physics and Chemistry of Solids*, 110 (2017) 254.
84. S. Luo, F. Qin, H. Zhao, Y. Liu and R. Chen, *Journal of hazardous materials*, 340 (2017) 253.
85. J. Liu, Y. Zhao, J. Ma, Y. Dai, J. Li and J. Zhang, *Ceramics International*, 42 (2016) 15968.
86. H. Li, Y. Zhang, C. Li, Z. Zhou, X. Nie, Y. Chen, H. Cao, B. Liu, N. Zhang and Z. Said, *Korean Journal of Chemical Engineering*, (2022) 1.
87. L. Feng, J.J. Liu, Z.C. Guo, T.Y. Pan, J.H. Wu, X.H. Li, B.Z. Liu and H.L. Zheng, *Separation and Purification Technology*, 285 (2021)120314.